

Improved CFA Interpolation Approach

R. Lukac, K.N. Plataniotis and D. Hatzinakos

*The Edward S. Rogers Sr. Department of ECE, University of Toronto
Toronto, Ontario, Canada*

B. Smolka

*Silesian University of Technology, Laboratory of Multimedia Communication
Rybnik, Poland*

Abstract

In this paper, a new color filter array (CFA) interpolation method for digital still cameras is introduced. Building on the computed edge-sensing map and a refined color difference model, a new correlation-correction algorithm is introduced. Due to edge-sensing interpolation mechanism and correction steps performed for each color channel, the proposed interpolation scheme is able to overcome the limitations of existing CFA based image acquisition solutions and restore color images without introducing false colors, edge blurring or visual artifacts. Moreover, the proposed method is described in a novel vector notation, which readily unifies previously developed schemes. Simulation studies indicate that the proposed method is computationally efficient and yields excellent performance, in terms of subjective and objective image quality measures, while outperforming well-known and widely used CFA interpolation methods.

Introduction

Digital color cameras acquire color information by transmitting the image through Red (R), Green (G) and Blue (B) color filters having different spectral transmittances and then sampling the resulted images using three electronic sensors, usually charge coupled devices (CCD) and complementary metal oxide semiconductor (CMOS) sensors.¹² To reduce cost and complexity, digital camera manufacturers use a single CCD/CMOS sensor with a color filter array (CFA) to capture all the three primary colors (R,G,B) at the same time. The Bayer pattern (Figure 1),² a widely used CFA, provides the array or mosaic of the RGB colors so that only one color element is available in each pixel, whereas two missing colors must be estimated from the adjacent pixels. This process is called CFA interpolation, or demosaicing.^{5,9,12,13}

This paper focuses on a new CFA interpolation method described in a novel vector notation of Ref. [12]. The proposed edge-sensing method improves color fidelity of restored images using a simple correction step based on a difference plane model.

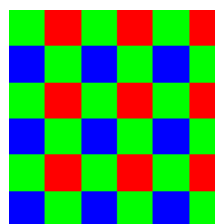


Figure 1. Bayer CFA pattern.

Proposed Method

Let us consider, a $K_1 \times K_2$ gray-scale image $z(i): Z^2 \rightarrow Z$ representing a two-dimensional matrix of integer samples. In the Bayer CFA pattern, half of the pixels z_i , for $i = 1, 2, \dots, K_1 K_2$, correspond to the G channel, whereas the R,B channels are assigned the other half of the pixels. Assuming that $p = 1, 2, \dots, K_1$ and $q = 1, 2, \dots, K_2$ denote the spatial position of the pixels in vertical (image rows) and horizontal (image columns) directions, gray-scale pixels z_i can be transformed into the RGB vectors $\mathbf{x}_i = (x_{i1}, x_{i2}, x_{i3})$, for $i = (p-1)K_2 + q$, as follows¹¹:

$$\mathbf{x}_i = \begin{cases} (z_i, 0, 0) & \text{for } p \text{ odd and } q \text{ even,} \\ (0, 0, z_i) & \text{for } p \text{ even and } q \text{ odd,} \\ (0, z_i, 0) & \text{otherwise.} \end{cases} \quad (1)$$

This transformation forms a $K_1 \times K_2$ RGB image $\mathbf{x}(i): Z^2 \rightarrow Z^3$ representing a two-dimensional matrix of three-component samples. Note that the color vectors \mathbf{x}_i relate to one true component varying in k from position to position, whereas other two components of \mathbf{x}_i are set to zero. Therefore, it is desirable to estimate the missing color components of the image $\mathbf{x}(i)$ and constitute the interpolated RGB image $\mathbf{y}(i): Z^2 \rightarrow Z^3$ to be as close to the desired RGB image $\mathbf{o}(i): Z^2 \rightarrow Z^3$ as possible.

To estimate the missing color components of $\mathbf{x}(i)$, a sliding supporting window $W = \{\mathbf{x}_i; i = 0, 1, \dots, N-1\}$ of finite size N is considered with the sample under consideration, sample \mathbf{x}_0 , placed in the center of the window (Figure 2). The procedure replaces \mathbf{x}_0 by some function of the local neighborhood area $\mathbf{x}_1, \mathbf{x}_2, \dots, \mathbf{x}_{N-1}$ at a time. The rationale of this approach is to minimize the local distortion and ensure the stationarity of the processes generating the image.^{10,14}

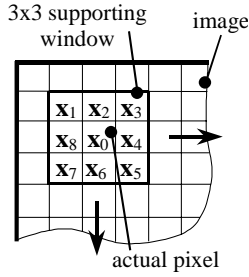


Figure 2. Sliding supporting window.

To follow structural information and interpolate missing image components in sharp shapes, efficient interpolation algorithms incorporate edge information into the interpolation process. A number of edge-detection mechanisms, which differentiate in preferred edge directions, have been introduced in the past years. The proposed method takes advantage of an 8-direction system of Ref. [8], which determines edge-sensing weight coefficients as follows:

$$w_1 = \frac{1}{1 + (|z_0 - z_9| + |z_1 - z_5|)/(2\sqrt{2})} \quad (2)$$

$$w_2 = \frac{1}{1 + (|z_0 - z_{11}| + |z_2 - z_6|)/2} \quad (3)$$

where w_1 and w_2 denote weights in north-west and north directions (Figure 3) and z_0, z_1, \dots, z_{24} are original gray-scale values of $z(i)$. Weights w_2, w_3, \dots, w_8 are calculated analogously to (2) and (3).

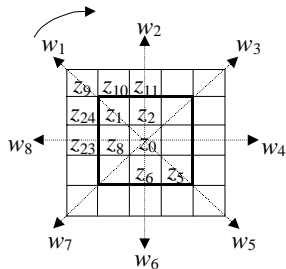


Figure 3. Edge-sensing scheme used in the proposed design.

Using the edge-sensing scheme shown in Figure 3, the G channel is adaptively interpolated as follows:

$$\bar{y}_{02} = \begin{cases} x_{02} & \text{if } z_0 \equiv x_{0k}, \\ \sum_{i=1}^{N-1} w'_i x'_{i2} & \text{otherwise} \end{cases} \quad (4)$$

where w'_1, w'_2, \dots, w'_8 are normalized weighting coefficients and x'_{i2} are pre-determined G values. For illustration purposes, $x'_{(1)2}$ and $x'_{(2)2}$ are given by

$$x'_{(1)2} = \frac{x_{(2)2} + x_{(8)2} + (z_1 - z_5)/(2\sqrt{2}) + (z_{11} - z_0 + z_{23} - z_0)/4}{2} \quad (5)$$

$$x'_{(2)2} = x_{(2)2} + (z_{11} - z_0 + z_2 - z_6)/4 \quad (6)$$

Note that $N=9$ relates to a 3×3 sliding window, z_0 is the acquired pixel before the transformation (1) in the same spatial position as the RGB vector x_i and operator \equiv denotes a one to one relationship.

Using the difference plane model¹ and the G values obtained in (4), the R,B channels are estimated as follows:

$$\bar{y}_{0k} = \begin{cases} x_{0k} & \text{if } z_0 \equiv x_{0k}, \\ \bar{y}_{02} + \sum_{i=1}^{(N-1)/2} w''_i (x_{(2i)k} - \bar{y}_{(2i)2}) & \text{if } z_0 \equiv x_{02}, \\ \bar{y}_{02} + \sum_{i=1}^{(N-1)/2} w''_i (x_{(2i-1)k} - \bar{y}_{(2i-1)2}) & \text{if } z_0 \equiv x_{0(k \pm 2)}, \end{cases} \quad (6)$$

where $k=1$ and $k=3$ characterize the R and B channels, respectively and $w''_1, w''_2, \dots, w''_4$ are the normalized weights corresponding to edges in north, east, south and west directions, whereas $w''_1, w''_2, \dots, w''_4$ are the weights corresponding to the diagonally positioned edges.

It has been observed^{8,9,11,12} that introducing a correction mechanism into the interpolation process improves contrast and accuracy of the initially interpolated G channel. Since the difference plane model of (6) is simple and efficient, it is also perfectly suited to a correction stage. Thus, the correction process related to the G channel is given by

$$y_{02} = \begin{cases} \bar{y}_{02} + \sum_{i=1}^{(N-1)/2} w''_i (\bar{y}_{(2i)2} - \bar{y}_{(2i)2}) & \text{if } z_0 \equiv x_{0k}, \\ \bar{y}_{02} & \text{otherwise} \end{cases} \quad (7)$$

where $w''_1, w''_2, \dots, w''_4$ are the same coefficients used in (6).

Considering the corrected G values of (7) the R,B update is completed using the following step:

$$y_{0k} = \begin{cases} x_{0k} & \text{if } z_0 \equiv x_{0k}, \\ y_{02} + \sum_{i=1}^{(N-1)/2} w''_i (\bar{y}_{(2i)2} - y_{(2i)2}) & \text{if } z_0 \equiv x_{02}, \\ y_{02} + \sum_{i=1}^{(N-1)/2} w''_i (\bar{y}_{(2i-1)2} - y_{(2i-1)2}) & \text{if } z_0 \equiv x_{0(k \pm 2)}, \end{cases} \quad (8)$$

Experimental Results

To examine the performance of the proposed framework and facilitate comparisons with the state of-the-art CFA interpolation schemes, some widely used natural test color images shown in Figure 4 are utilized. All test images have been normalized to a standard size of 512×512 pixels with a 8-bit per channel RGB representation.

The proposed method is compared with other CFA interpolation methods, such as bilinear interpolation (BI),¹³ bilinear difference (BD) approach,¹³ color correlations-directional derivatives method (C2D2),⁸ Kimmel algorithm (KA) [9], alternating projections (AP) approach,⁵ saturation-based adaptive inverse gradient interpolation (SAIG),³ median filter interpolation (MFI),⁴ high definition color interpolation scheme (EMI)⁷ and adaptive color plane interpolation (API),⁶ which is currently used in digital cameras.

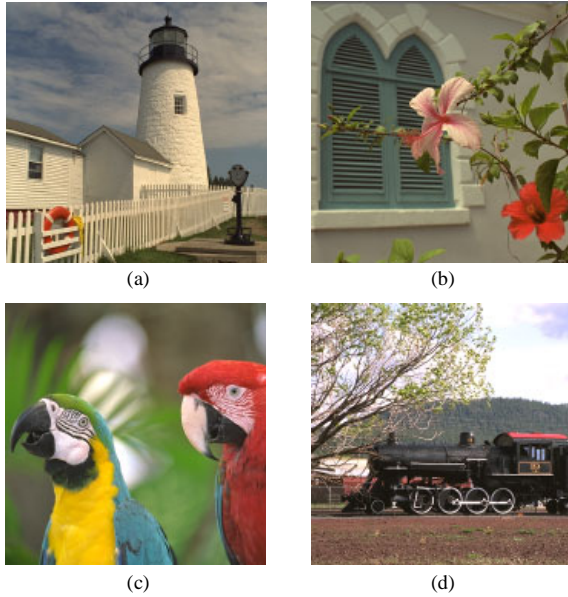


Figure 4. Test color images: (a) Lighthouse, (b) Window, (c) Parrots, (d) Train.

To measure similarity between the original, full RGB, image $\mathbf{o}(i)$ and interpolated image $\mathbf{y}(i)$, a number of different objective measures, based on the difference in the statistical distributions of the pixel values, can be utilized.¹⁰ In this paper, the mean square error (MSE) and the normalized color difference (NCD) are used to measure objectively the quality of the restored RGB image.

The MSE criterion is defined as follows:

$$\text{MSE}_k = \frac{1}{K_1 K_2} \sum_{i=1}^{K_1 K_2} (o_{ik} - y_{ik})^2 \quad (9)$$

where $\mathbf{o}_i = (o_{i1}, o_{i2}, o_{i3})$ is the original pixel, $\mathbf{y}_i = (y_{i1}, y_{i2}, y_{i3})$ is the restored pixel, i denotes the pixel position in a $K_1 \times K_2$ color image and k characterizes the color channel.

To quantify the perceptual closeness between the original and the obtained solution, the NCD criterion is used in this work. The NCD is given by

$$\text{NCD} = \frac{\sum_{i=1}^{K_1 K_2} \sqrt{(L_{o_i}^* - L_{y_i}^*)^2 + (u_{o_i}^* - u_{y_i}^*)^2 + (v_{o_i}^* - v_{y_i}^*)^2}}{\sum_{i=1}^{K_1 K_2} \sqrt{(L_{o_i}^*)^2 + (u_{o_i}^*)^2 + (v_{o_i}^*)^2}} \quad (10)$$

where L^* represents lightness values and u^*, v^* chrominance values corresponding to original \mathbf{o}_i and restored \mathbf{y}_i samples expressed in CIELUV color space.

Tables 1-4 summarize results corresponding to the restoration of test images shown in Figure 4. Using natural test images we are able to compare performance of the methods in realistic applications, since in these images the correlation between the color channels vary significantly. It can be seen that the flexible design characteristics of the proposed method result in excellent performance as the reported error values indicate.

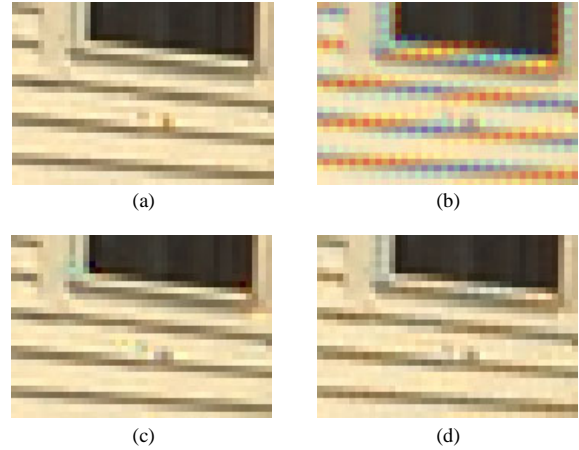


Figure 5. Zoomed parts of the test image Lighthouse: (a) original image, (b) BI, (c) API, (d) proposed method.

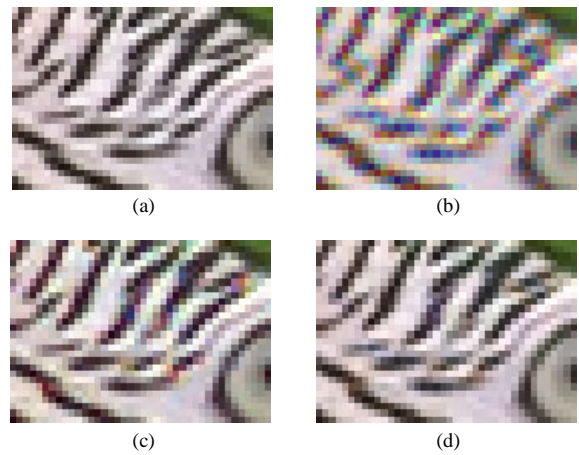


Figure 6. Zoomed parts of the test image Parrots: (a) original image, (b) BI, (c) API, (d) proposed method.

Figure 5 and Figure 6 present zoomed parts of the restored images. These images allow for the comparison of the results corresponding to the fundamental BI and currently used API technique with those obtained through the proposed method in terms of a subjective (user-centered) evaluation. It is evident that the BI scheme fails near edges and produces color artifacts. The API scheme produces more quality results. It can be seen that the proposed method is capable of restoring the color images with a high visual quality and avoids color shifts and visual artifacts. Clearly, the proposed framework produces impressive visual quality of the restored images shown in Figure 5d and Figure 6d.

Table 1. Comparison using the test image Lighthouse

Method	MSE _R	MSE _G	MSE _B	NCD
BI	138.69	44.32	134.23	0.0653
BD	23.24	12.65	21.91	0.0321
C2D2	16.94	13.16	17.57	0.0301
KA	16.97	16.38	26.35	0.0317
AP	9.15	4.74	7.40	0.0237
SAIG	109.40	16.71	107.04	0.0588
MFI	44.28	7.94	40.78	0.0380
EMI	21.83	16.36	29.56	0.0370
API	14.57	9.71	13.19	0.0298
Proposed	10.30	5.25	9.95	0.0236

Table 2. Comparison using the test image Window

Method	MSE _R	MSE _G	MSE _B	NCD
BI	41.48	17.24	41.61	0.0417
BD	7.06	4.57	7.92	0.0228
C2D2	6.19	5.67	6.70	0.0193
KA	11.69	10.10	12.59	0.0256
AP	6.16	3.38	6.61	0.0212
SAIG	23.95	7.57	23.50	0.0322
MFI	9.50	2.88	9.78	0.0239
EMI	12.42	9.80	11.33	0.0252
API	7.03	4.53	7.11	0.0209
Proposed	4.88	2.27	5.52	0.0181

Table 3. Comparison using the test image Parrots

Method	MSE _R	MSE _G	MSE _B	NCD
BI	34.858	14.935	38.251	0.0262
BD	4.876	4.059	8.415	0.0170
C2D2	5.446	5.242	7.099	0.0162
KA	12.577	9.584	9.743	0.0190
AP	4.588	3.806	8.151	0.0167
SAIG	22.138	7.562	24.450	0.0229
MFI	7.090	2.909	10.433	0.0172
EMI	20.344	17.696	10.553	0.0207
API	5.403	4.285	7.895	0.0173
Proposed	3.909	2.490	6.261	0.0152

Table 4. Comparison using the test image Train

Method	MSE _R	MSE _G	MSE _B	NCD
BI	517.71	254.59	607.19	0.1450
BD	74.71	65.45	113.47	0.0744
C2D2	93.30	113.51	128.97	0.0702
KA	71.22	85.68	138.41	0.0641
AP	44.43	30.80	78.39	0.0560
SAIG	387.31	162.39	456.27	0.1246
MFI	115.44	46.03	163.34	0.0798
EMI	159.42	152.53	195.69	0.0845
API	109.24	96.62	145.01	0.0776
Proposed	40.44	31.24	71.69	0.0503

Conclusion

The presented edge-sensing CFA interpolation method performed interpolation and correction steps based on a color difference model. Therefore, the proposed method follows structural image information and makes the interpolated images sharp, naturally colored and pleasurable for viewing. This also produces excellent results in terms of commonly used objective criteria. Achieved results indicate that the proposed method is sufficiently robust and significantly outperforms state-of-the-art CFA interpolation.

References

1. J. Adams, Design of Practical Color Filter Array Interpolation Algorithms for Digital Cameras, Proc. of the SPIE, 3028, pp. 117-125 (1997).
2. B.E. Bayer, Color Imaging Array, U.S. Patent 3 971 065, 1976.
3. C. Cai, T.H. Yu, and S.K. Mitra, "Saturation-based adaptive inverse gradient interpolation for Bayer pattern images, IEE Proc. - Vision, Image, Signal Processing, 148, pp. 202-208 (2001).
4. W.T. Freeman, Median Filter for Reconstructing Missing Color Samples, U.S. Patent 5 373 322, 1988.
5. B. Gunturk, Y. Altunbasak, and R. Mersereau, Color Plane Interpolation Using Alternating Projections, IEEE Trans. Image Processing, 11, pp. 997-1013 (2002).
6. J.F. Hamilton and J.E. Adams, Adaptive Color Plane Interpolation in Single Sensor Color Electronic Camera, U.S. Patent 5 629 734, 1997.
7. B.S. Hur and M.G. Kang, High Definition Color Interpolation Scheme for Progressive Scan CCD Image Sensor, IEEE Trans. Consumer Electronics, 47, pp. 179-186, (2001).
8. N. Kehtarnavaz, H.J Oh, and Y. Yoo, Color Filter Array Interpolation Using Color Correlations and Directional Derivatives, Journal of Electronic Imaging, to appear (2003).
9. R.Kimmel, Demosaicing: Image Reconstruction from Color CCD Samples, IEEE Trans. Image Processing, 8, pp. 1221-1228, (1999).
10. R. Lukac, B. Smolka, K. Martin, K.N. Plataniotis, and A.N. Venetsanopoulos, Vector Filtering for Color Imaging, IEEE Signal Processing Magazine, Special Issue on Color Image Processing, to appear (2004).
11. R. Lukac and K.N. Plataniotis, A New Color Restoration Solution for Bayer Pattern Based Imaging Devices, IEEE Signal Processing Letters, to appear (2004).
12. R. Lukac, K.N. Plataniotis, D. Hatzinakos, and M. Aleksic, A New CFA Interpolation Framework, Signal Processing, submitted for publication (2003).
13. S.C. Pei and I.K. Tam, Effective Color Interpolation in CCD Color Filter Arrays Using Signal Correlation, IEEE Trans. Circuits and Systems for Video Technology, 13, pp. 503-513 (2003).
14. K.N. Plataniotis and A.N. Venetsanopoulos, Color Image Processing and Applications. Springer Verlag, 2000.

lukacr@ieee.org, kostas@dsp.utoronto.ca